
Fourier Continuation for Exact Derivative Computation in Physics-Informed Neural Operators

Haydn Maust Zongyi Li Yixuan Wang Daniel Leibovici
 Oscar Bruno Thomas Hou Anima Anandkumar
 California Institute of Technology
 {hmaust, zongyili, roywang, dleibovi, obruno, anima}@caltech.edu
 hou@cms.caltech.edu

Abstract

The physics-informed neural operator (PINO) is a machine learning architecture that has shown promising empirical results for learning partial differential equations. PINO uses the Fourier neural operator (FNO) architecture to overcome the optimization challenges often faced by physics-informed neural networks. Since the convolution operator in PINO uses the Fourier series representation, its gradient can be computed exactly on the Fourier space. While Fourier series cannot represent nonperiodic functions, PINO and FNO still have the expressivity to learn nonperiodic problems with Fourier extension via padding. However, computing the Fourier extension in the physics-informed optimization requires solving an ill-conditioned system, resulting in inaccurate derivatives which prevent effective optimization. In this work, we present an architecture that leverages Fourier continuation (FC) to apply the exact gradient method to PINO for nonperiodic problems. This paper investigates three different ways that FC can be incorporated into PINO by testing their performance on a 1D blowup problem. Experiments show that FC-PINO outperforms padded PINO, improving equation loss by several orders of magnitude, and it can accurately capture the third order derivatives of nonsmooth solution functions.

1 Introduction

Machine learning has recently seen widespread applications in approximating solutions to partial differential equations. Physics-Informed Neural Networks (PINNs) [1–3] can learn solutions to partial differential equations with little or no ground-truth solution data. A neural network as the ansatz of the solution function is used to take advantage of auto-differentiation [4] to compute the exact, mesh-free derivatives. Recent advances in PINNs show successful attempts on 1D and 2D blowup problems [5]. While PINNs are flexible and easy to use, they face several optimization issues when applied to nonlinear PDEs due to the highly nonsmooth and nonconvex optimization [6–10]. A more recent architecture known as the Physics-Informed Neural Operator (PINO) [11, 12] empirically outperforms PINNs on many learning tasks. PINO uses the neural operator model as the ansatz, which has an easier optimization landscape and a more expressive representation space compared to the neural network ansatz used by PINNs. The neural operator parameterizes the solution function as an aggregation of basis functions, and hence, the optimization is in function space. This is easier than just optimizing a single function as in PINNs.

Computing the equation loss of a model output requires taking the derivative of that output. Since PINO presents the output function as projected Fourier series, its gradients can be exactly computed on the Fourier space, similar to conventional Fourier methods. However, because PINO uses Fourier series representation, the exact gradient can only be applied to periodic functions; using finite Fourier

series on a nonperiodic function causes a Gibbs phenomenon, leading to poor optimization as shown in the fifth row of Figure 4. One simple alternative is to use the Fourier series on a larger domain by padding or expanding the original domain (for example, using the half-range Fourier series). Such extension grants FNO and PINO the expressivity for general nonperiodic problems. However, there is a severe ill-conditioning issue [13] since the discrete Fourier transform is a Vandermonde matrix [14]. To apply the Fourier method to problems with nonperiodic solutions, one must convert the model output to a periodic form in a well-conditioned manner. Fourier continuation (FC) methods [15–17] continue the nonperiodic model output into a periodic function on an extended domain using lower-order polynomials. Numerically, conventional FC methods have shown a superalgebraic convergence rate. Therefore, we propose Fourier continuation as a solution that enables PINO to be applied to nonperiodic functions while retaining numerical precision.

This paper investigates three different ways that Fourier continuation can be incorporated into PINO (FC only at the end of the model, FC in each Fourier layer, and FC at the beginning with truncation at the end). We compare the performance of each model on the self-similar Burgers’ equation, which is a 1D differential equation with a nonsmooth solution for some parameter values. We find that the best-performing architecture uses Fourier continuation only at the end of the model just before using the exact gradient method to compute derivatives, and not in any of the intermediate layers. From a theoretical perspective, this is because in architectures with FC in intermediate layers, the hidden layers act on an extended domain while the model is only optimized on the base domain; this “partially observed optimization” leads to optimization problems that empirically result in the final model oscillating around the ground truth solution, especially near the boundary. PINO with Fourier continuation in the last layer shows strong empirical results even when learning nonsmooth solution functions, which suggests that Fourier continuation is an effective approach to applying PINO in aperiodic settings.

2 Background

2.1 PINNs and PINOs

Physics-Informed Neural Networks (PINNs) [1] are a neural network learning algorithm that, in addition to the agreement with training data points, incorporates adherence to physical constraints into the network’s loss function. For a stationary system, a PINN learns an approximation u_θ to the solution u to a partial differential equation

$$\begin{aligned} \mathcal{P}(u, a) &= 0, & \text{in } D \subset \mathbb{R}^d \\ u &= g, & \text{in } \partial D \end{aligned}$$

where \mathcal{P} is a differential operator, a is a coefficient, and g is a boundary condition. In this case, the loss term has the following form [11], where $\alpha \in \mathbb{R}^+$ is a constant:

$$\mathcal{L}_{\text{pde}}(a, u_\theta) = \int_D |\mathcal{P}(u_\theta(x), a(x))|^2 dx + \alpha \int_{\partial D} |u_\theta(x) - g(x)|^2 dx. \quad (1)$$

The integrals over D and ∂D measure how close the prediction u_θ is to satisfying the constraints $\mathcal{P}(u_\theta, a) = 0$ and $u_\theta|_{\partial D} = g$ respectively. PINNs have shown promising results in empirical trials, achieving small errors without overfitting even when trained on datasets on the order of only 50 points [1].

An architecture closely related to PINNs is the Physics-Informed Neural Operator (PINO). The neural operator is an architecture that learns maps between infinite-dimensional vector spaces, such as function spaces, rather than between finite-dimensional vector spaces [18]. The neural operator has the following form [11]:

$$\mathcal{G}_\theta := \mathcal{Q} \circ (W_L + \mathcal{K}_L) \circ \cdots \circ \sigma(W_1 + \mathcal{K}_1) \circ \mathcal{P}. \quad (2)$$

Here \mathcal{P} , \mathcal{Q} are neural networks that map a low-dimensional function into high-dimensional space and vice versa. Each intermediate layer consists of a matrix W_l , an integral kernel operator \mathcal{K}_l , and an activation function σ . In this paper we use the Fourier neural operator [19], which means that the integral kernel operators \mathcal{K}_l are linear transformations in frequency space. In other words, these operators have the form

$$\mathcal{K}_l = \mathcal{F}^{-1} \circ A_l \circ \mathcal{F},$$

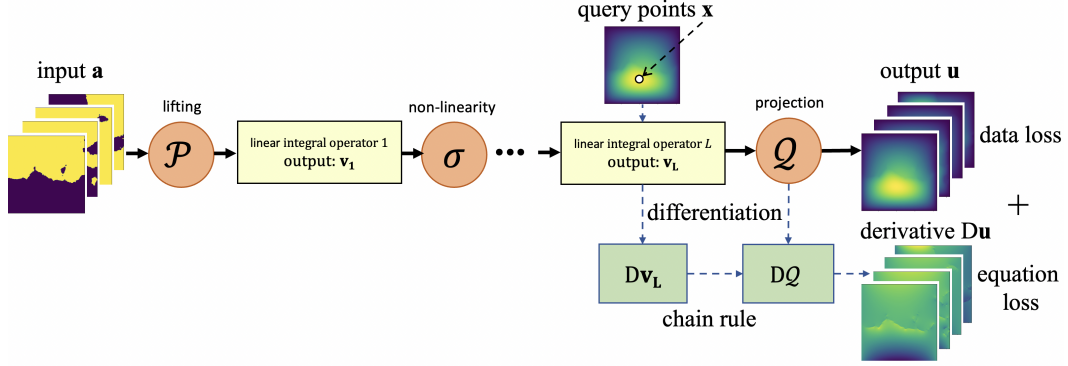


Figure 1: A diagram of the Fourier neural operator architecture, adapted from [11]. Each linear integral layer is given by a Fourier convolution term plus a skip connection term ($W_l + \mathcal{K}_l$), followed by the activation function σ . The exact derivatives are computed on the Fourier space and composed with the projection.

where A_l are matrices to be optimized and $\mathcal{F}, \mathcal{F}^{-1}$ are the fast Fourier transform and its inverse. To compute derivatives, we take the model output before applying \mathcal{Q} and use FFT to take the derivative in frequency space. From there, one can explicitly apply the chain rule for the neural network layer \mathcal{Q} to obtain the final model derivative. A diagram of the architecture is shown in Figure 1. One advantage of neural operators over traditional neural networks is that the parameters learned by neural operators are independent of the discretization of the input space, meaning that parameters learned at one resolution can be applied at a different resolution [20]. Similar to PINNs, PINOs incorporate physical constraints into the loss function of the neural operator, making it more viable to train on small datasets, or even no dataset at all [11]. PINOs have shown substantial improvements in both speed and accuracy compared to PINNs.

One current application area of PINO methods is modeling blowups in fluid equations. Proving that fluid equations blow up in finite time under certain initial conditions is an area of interest for theoretical work, but empirical methods can also aid in the search for blowups. Modeling blowup is useful because it identifies approximate candidates for blowups. If we can bound the error on these blowup candidates, then linear/nonlinear stability is sufficient to conclude that blowup does actually occur at a perturbation around the blowup candidate; see [8, 21]. As a result, improving the accuracy of PINO models is key for proving blowups.

2.2 Fourier continuation

When using PINO to model solutions to differential equations, the ability to compute derivatives with high accuracy is key. PINO uses the exact gradient method where the gradient is computed in Fourier space as shown in Figure 1. The challenge that comes with using the exact gradient method is that the Fourier series is only well-defined for periodic functions. To apply it to problems with nonperiodic solutions, one must convert the nonperiodic model output to a periodic form. The most straightforward way to extend the domain is known as padding or Fourier extension. In this regime, the model outputs a periodic function on the extended domain, but only the subset of the domain relevant to the problem is used for optimization. For example, to find a nonperiodic function on the interval $[0, L]$, one would train a model that outputs functions on $[-L, L]$, but use only the output on $[0, L]$ for optimization and ignore the output on $[-L, 0]$. However, this padding method is a so-called partially observed optimization problem: one is optimizing a model that outputs on $[-L, L]$, but the loss is only computed from the outputs on $[0, L]$.

The PINO model uses the Fourier integral layers \mathcal{K}_l , which require taking Fourier transforms. The discrete Fourier transform operator is described by an ill-conditioned Vandermonde matrix, meaning that the ratio of the matrix's largest eigenvalue to its smallest eigenvalue is very large. As a result, optimization problems that involve the Fourier transform, such as learning a function on a fixed domain by performing least-squares optimization of Fourier coefficients, lead to ill-conditioning

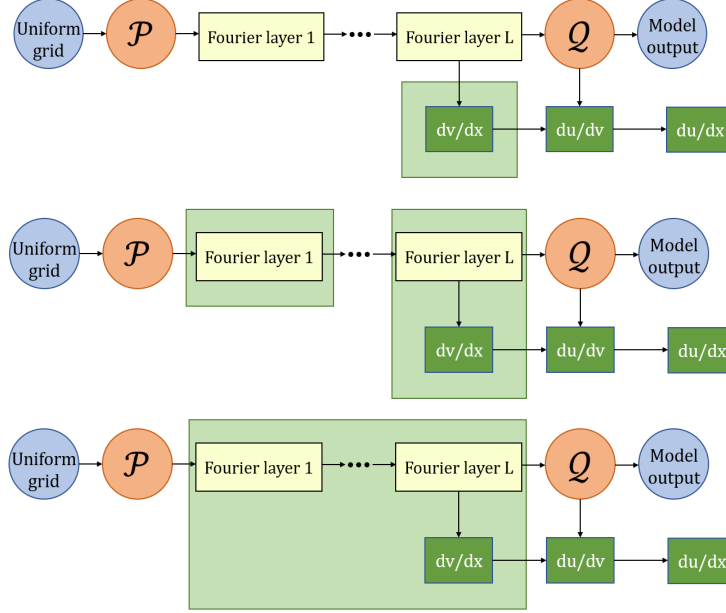


Figure 2: Diagrams of the FC-PINO models 1 (top), 2 (middle), and 3 (bottom). The light green highlighted regions indicate where Fourier continuation is used: entering a green highlighted region means applying FC, and exiting a region means truncating to the base domain.

problems. For a simplified formulation, consider the linear system

$$\mathcal{F}^{-1}A = B.$$

If such a system is partially observed, the optimization process becomes very sensitive to small numerical errors. Small perturbations in B will cause huge errors in A ; see Fig. 3 in [22]. This ultimately makes gradient-descent optimization infeasible. To find a more stable solution, it is necessary to use an architecture that is not ill-conditioned.

To extend nonperiodic functions to periodic ones, the alternative to padding is deterministic continuation methods. These methods use function outputs on the original domain to produce a periodic continuation on the extended domain with lower-order polynomials. In the next section, we examine several PINO architectures that implement the exact gradient method with deterministic continuation and compare the results from each architecture.

3 FC-PINO

The basic neural operator architecture is given in equation (2). We consider three PINO models that incorporate FC. Diagrams of each model are shown in Figure 2.

Model 1 uses FC merely as a computational tool to compute derivatives. The final layer Q is a simple neural network, so its derivative is straightforward to compute directly. Given the derivative of the rest of the model before Q , one can compute the derivative of the entire model output \mathcal{G}_θ with the chain rule. To compute the derivative of the model output before Q , we use FC to extend the output to a periodic function, take the derivative using the exact gradient method, then truncate to the original domain. Model 1 has the same structure as the base neural operator given in equation (2), except that FC is used in the derivative computation between the last Fourier layer and Q .

$$\mathcal{G}_1 := Q \circ R \circ \text{FC} \circ (W_L + \mathcal{K}_L) \circ \cdots \circ \sigma(W_1 + \mathcal{K}_1) \circ \mathcal{P}. \quad (3)$$

Model 2 is identical to Model 1 except that FC is also applied in the Fourier kernel operators \mathcal{K}_l . Let FC denote the operation of Fourier continuation onto an extended domain and let R denote restriction back to the base domain. Following the format of equation (2), we can write model 2 as follows:

$$\mathcal{G}_2 := Q \circ (W_L + R \circ \mathcal{K}_L \circ \text{FC}) \circ \cdots \circ \sigma(W_1 + R \circ \mathcal{K}_1 \circ \text{FC}) \circ \mathcal{P}. \quad (4)$$

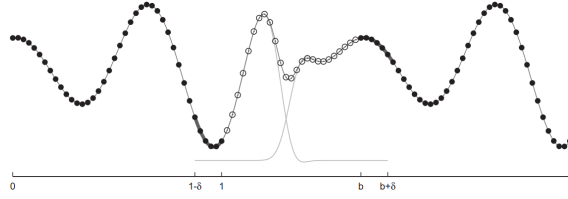


Figure 3: An illustration of the Fourier continuation method. The points in $[0, 1]$ are the original function, and the points in $(1, b)$ are the continuation. Image adapted from [15].

Thus each Fourier kernel operator is applied to a periodic function on the extended domain.

Model 3 applies FC to the output of the initial neural network \mathcal{P} , then truncates the domain before \mathcal{Q} . We can write model 3 as follows:

$$\mathcal{G}_3 := \mathcal{Q} \circ R \circ (W_L + \mathcal{K}_L) \circ \cdots \circ \sigma(W_1 + \mathcal{K}_1) \circ \text{FC} \circ \mathcal{P}. \quad (5)$$

The FC after \mathcal{P} makes the model periodic, so each intermediate layer acts on a periodic function. As a result, the output before \mathcal{Q} is still periodic, so we can apply the exact gradient method to compute derivatives.

The deterministic continuation function that we will use is the FC-Gram method described in [15]. FC-Gram uses a small number of gridpoints near the boundary of the base domain and interpolates those points by trigonometric polynomials that are periodic on an extended domain, hence producing a continuation [22]. Empirically, the trigonometric polynomial interpolation has a very small error when compared against the original function on the base domain [22]. An illustration of the FC-Gram procedure is shown in Figure 3.

FC-Gram gives a continuation that is k times differentiable at the transition points between the base domain and the extended domain, where one can choose the value of k . Large k leads to very smooth continuations. However, these continuations also suffer from an ill-conditioning problem: a 5th-order derivative continuation is very sensitive to small changes in the original function values because small changes in the function can cause much larger changes in the 5th derivative. As a result, using high-order Fourier continuation often causes the learned model to exhibit oscillation near the boundary of the base domain; see Figure 8 in appendix C for an example. On the other hand, small values of k lead to continuations that have discontinuities in the second- or third-order derivatives. Since PDE models use these higher-order derivatives in the optimization process, it is important that these derivatives be continuous to avoid numerical precision problems. For this paper, we use $k = 3$ for all Fourier continuation methods to balance the drawbacks of small and large values of k .

4 Numerical Results

4.1 Problem Setting

Recall the base neural operator architecture from (2), which produces nonperiodic outputs. There are several places to introduce Fourier continuation into the model that enables the exact gradient method for taking derivatives. In this section, we will list some of these choices, compare the performance of each resulting model, and attempt to explain the performance differences using ill-conditioning theory. To simplify experiments, we work with one-dimensional problems. Fortunately, the 1D case has a useful toy problem for model testing. We begin with the non-viscous Burgers' equation

$$u_t + uu_x = 0$$

where $u(x, t)$ is the solution function. From there, if we make the substitution

$$u = (1 - t)^\lambda U\left(\frac{x}{(1 - t)^{1+\lambda}}\right)$$

for some fixed $\lambda \in \mathbb{R}^+$, then the equation simplifies to

$$-\lambda U + ((1 + \lambda)y + U)U_y = 0 \quad (6)$$

	Training loss		L^2 loss	
	$\lambda = 0.4$	$\lambda = 0.5$	$\lambda = 0.4$	$\lambda = 0.5$
Model 1 (FC only at the end)	$10^{-8.4}$	$10^{-7.7}$	$10^{-6.1}$	$10^{-6.0}$
Model 2 (FC in each Fourier layer)	$10^{-6.5}$	$10^{-7.3}$	$10^{-6.1}$	$10^{-6.0}$
Model 3 (FC after \mathcal{P} , truncation before \mathcal{Q})	$10^{-5.5}$	$10^{-6.6}$	$10^{-6.1}$	$10^{-6.0}$
Baseline 1 (PINO on padded domain)	$10^{-2.5}$	$10^{-3.9}$	$10^{-5.3}$	$10^{-5.6}$
Baseline 2 (PINO with no continuation)	$10^{+2.3}$	$10^{+2.3}$	$10^{-0.5}$	$10^{-0.5}$

Table 1: First two columns: losses computed from equation (7) for models 1, 2, and 3 after 60,000 training epochs. Last two columns: L^2 losses (defined as in section A.1) of the output of each model against the exact solution to equation (6). For comparison, we also include two baselines: PINO on a padded domain as described in section 2.2, and PINO with no continuation.

where U is the solution function and U_y is the partial derivative of U with respect to y . Equation (6) is known as the self-similar Burgers’ equation. In this form, there is only one input variable y , so this is a 1D problem that can be solved with PINO. Furthermore, if we impose the boundary condition $U(-2) = 1$, then the solution to (6) is known to satisfy the equation

$$y = -U - U^{1+1/\lambda}$$

so any model outputs can easily be compared against the ground truth. We will compare models by evaluating their performance when trained on equation (6). Across each model we fix hyperparameters such as the number of layers and number of frequency modes used in the Fourier convolution layers \mathcal{K}_l as well as training parameters such as learning rate and the number of training epochs; see appendix B for details. Motivated by the results in [5], we also introduce an additional loss term to (1) which is the L^2 norm of the derivative with respect to y of the left side of (6), in order to model the smoothness of the solution. Hence the final loss expression is

$$\begin{aligned} \mathcal{L}_{\text{pde}}(a, u_\theta) &= \int_D |\mathcal{P}(u_\theta(x), a(x))|^2 dx + \alpha \int_{\partial D} |u_\theta(x) - g(x)|^2 dx + \beta \int_D \left| \frac{\partial}{\partial x} \mathcal{P}(u_\theta(x), a(x)) \right|^2 dx. \end{aligned} \quad (7)$$

The three terms correspond to equation loss, boundary loss, and smoothness loss respectively. For these experiments, we fix $\alpha = 100$ and $\beta = 1$.

4.2 Comparison across Different Architectures of Fourier Continuation

The final function plots for each of these models are shown in Figure 4. After 60,000 epochs, the losses computed from equation (7) are given in Table 1. Each of the models exhibits some amount of oscillation away from the exact solution when we look at the third derivative plots.

The two baseline models, given by (Baseline 1) padding the domain and (Baseline 2) using no continuation at all, are shown in the fourth and fifth rows respectively. As expected based on the discussion in section 2.2, Baseline 1 with padding performs poorly due to ill-conditioning from a partially observed optimization problem that involves Fourier coefficients. Baseline 2 with no continuation computes the derivative in Fourier space to fit a nonperiodic function; in other words, the derivative is computed by first applying FFT and then computing the derivative in frequency space. Applying FFT and then IFFT converts the model to a Fourier series, which leads to a Gibbs phenomenon at the boundary. As a result, the derivatives computed by this method are inaccurate, so the model ultimately optimizes based on an incorrect derivative in equation (7). This explains the poor performance of the model with no continuation.

For both $\lambda = 0.4$ and $\lambda = 0.5$, we see from the plots that model 3 has the largest oscillation. From Table 1, model 3 also has the largest loss values. The theoretical reason for this result is that model 3 effectively produces a partially-observed optimization problem. All of the layers between \mathcal{P} and \mathcal{Q} act on a periodic function defined on an extended domain. However, at the end, the model output is truncated before computing loss. This means that model 3 produces a function on an extended domain, but is only trained on a subset of that domain during optimization. As a result, the structure of

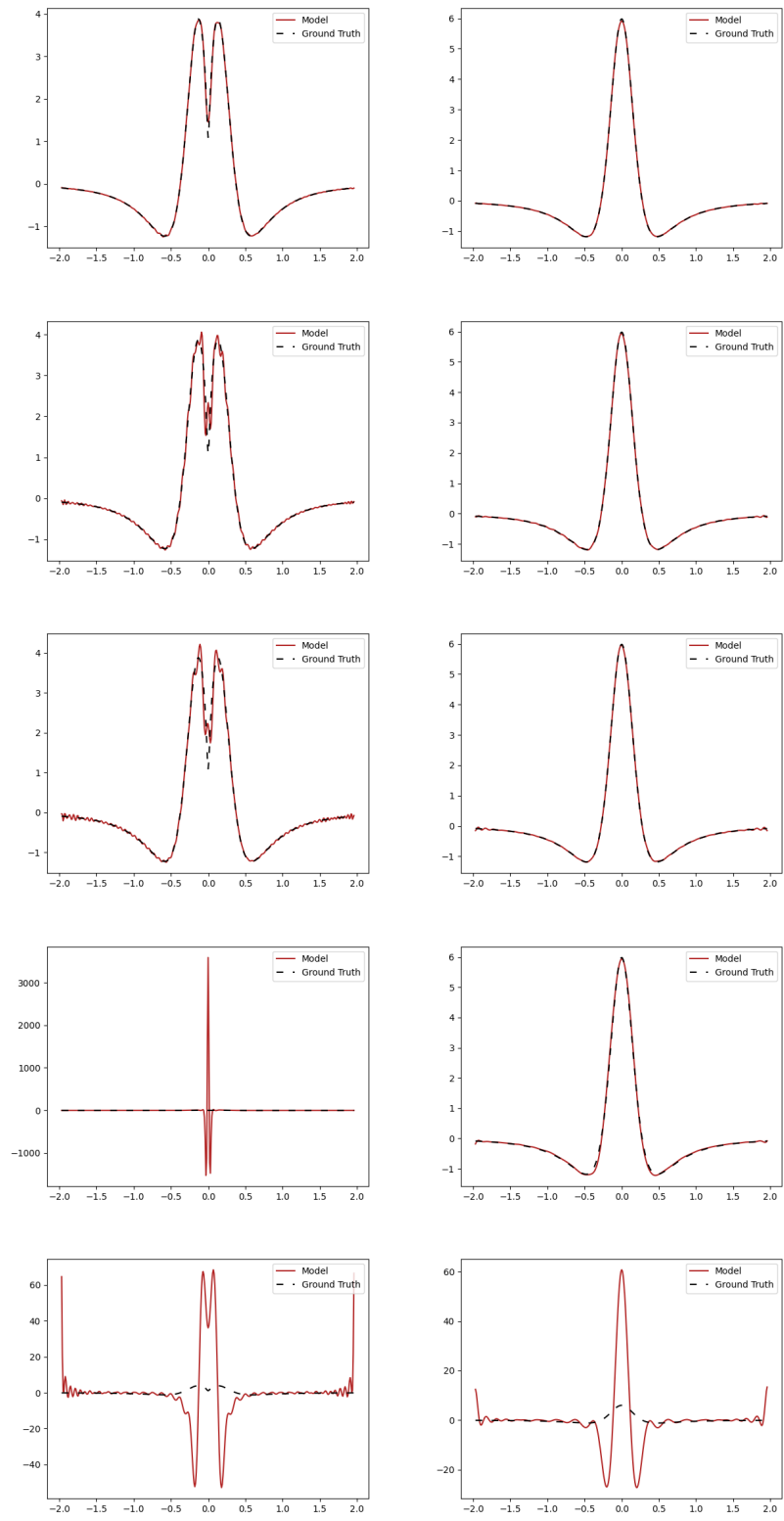


Figure 4: Plots of models 1 (first row), 2 (second row), and 3 (third row), as well as PINO on a padded domain (fourth row) and PINO with no continuation (fifth row), trained on equation (6) for 60,000 epochs with constants $\lambda = 0.4$ (left) and $\lambda = 0.5$ (right). To make the performance differences visually apparent, these plots show the third derivative of each model output.

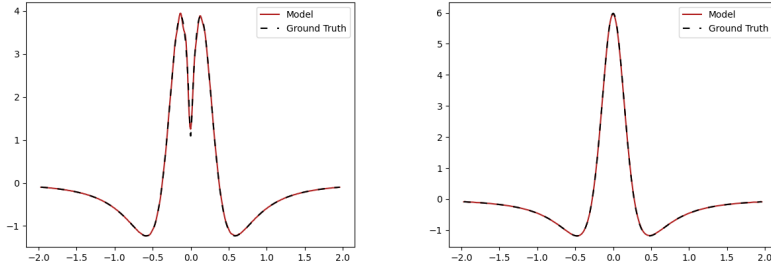


Figure 5: Third derivative plots of model 1 with additional adjustments trained on equation (6) for 60,000 epochs with constants $\lambda = 0.4$ (left) and $\lambda = 0.5$ (right).

model 3 implicitly produces a partially observed optimization problem, which causes ill-conditioning as described in section 2.2. Although model 2 only passes functions on the original domain between each layer, each Fourier kernel operator \mathcal{K}_l acts on an extended domain. This may produce some partially observed optimization problems as well, which explains the oscillation in the model 2 plots. On the other hand, the parametrized components of model 1 do not act on the extended domain; instead, FC is used only at the end to compute derivatives. Therefore model 1 does not create a partially observed optimization problem, and hence it performs the best out of the three models.

4.3 Results on the Self-Similar Burgers' Equation

In the experiments in section 4, we found that model 1 had the best performance on equation (6). We can introduce a few additional adjustments to the model to further improve its performance. First, recall that the Fourier kernel operators have the form $\mathcal{K} = \mathcal{F}^{-1} \circ A \circ \mathcal{F}$. In practice, we parametrize A as a finite-dimensional matrix, meaning that we only include a finite number of frequencies. Increasing the number of included frequencies enables the model to learn higher-frequency components of solution functions, such as the cusp in the third derivative of the solution to equation (6) when $\lambda = 0.4$. Including more high-frequency components can make the training process more unstable, so there is a tradeoff between expressiveness and stability. Second, it is straightforward to show that the solution to the self-similar Burgers' equation is odd. As a result, once we impose $U(-2) = 1$, we also know $U(2) = -1$. We can make the solution function 0th-order periodic by adding $0.5y$ to it. Training the PINO on this line-adjusted solution function is easier because we create 0th-order periodicity and the Fourier kernel layers are naturally periodic operators.

Applying these two adjustments and training model 1 for the constants $\lambda = 0.4$ and $\lambda = 0.5$, we obtain the plots in Figure 5. Plots of the original model output and its first and second derivatives are shown in Figure 9 in appendix C. Here the losses for $\lambda = 0.4$ and $\lambda = 0.5$ are $10^{-8.7}$ and $10^{-8.1}$ respectively.

5 Acknowledgements

H. Maust gratefully acknowledges the support of the Lynn A. Booth and Kent Kresa SURF Fellowship. Z. Li gratefully acknowledges the financial support from the Kortschak Scholars, PIMCO Fellows, and Amazon AI4Science Fellows programs. Oscar P. Bruno and Daniel Leibovici gratefully acknowledge support from NSF, AFOSR, and ONR through contracts DMS-2109831, FA9550-21-1-0373, and N00014-16-1-2808. T. Y. Hou is in part supported by the NSF grant DMS-2205590, the Choi Family Gift Fund, and the Charles Lee Powell endowed chair. A. Anandkumar is supported in part by Bren endowed chair.

References

1. Raissi, M., Perdikaris, P. & Karniadakis, G. E. Physics-informed neural networks: A deep learning framework for solving forward and inverse problems involving nonlinear partial differential equations. en. *Journal of Computational Physics* **378**, 686–707 (Feb. 2019).
2. Sirignano, J. & Spiliopoulos, K. DGM: A deep learning algorithm for solving partial differential equations. *Journal of computational physics* **375**, 1339–1364 (2018).
3. Yu, B. *et al.* The deep Ritz method: a deep learning-based numerical algorithm for solving variational problems. *Communications in Mathematics and Statistics* **6**, 1–12 (2018).
4. Baydin, A. G., Pearlmutter, B. A., Radul, A. A. & Siskind, J. M. Automatic Differentiation in Machine Learning: a Survey. en. *Journal of Machine Learning Research* **18**, 43 (2018).
5. Wang, Y., Lai, C.-Y., Gómez-Serrano, J. & Buckmaster, T. Asymptotic self-similar blow up profile for 3-D Euler via physics-informed neural networks. arXiv:2201.06780 [physics] type: article (Mar. 2022).
6. Wang, S., Teng, Y. & Perdikaris, P. Understanding and mitigating gradient flow pathologies in physics-informed neural networks. *SIAM Journal on Scientific Computing* **43**, A3055–A3081 (2021).
7. Fuks, O. & Tchelepi, H. A. Limitations of physics informed machine learning for nonlinear two-phase transport in porous media. *Journal of Machine Learning for Modeling and Computing* **1** (2020).
8. Chen, J., Hou, T. Y. & Huang, D. On the finite time blowup of the De Gregorio model for the 3D Euler equations. *Communications on pure and applied mathematics* **74**, 1282–1350 (2021).
9. Matthey, R. & Ghosh, S. A Physics Informed Neural Network for Time-Dependent Nonlinear and Higher Order Partial Differential Equations. *Computer Methods in Applied Mechanics and Engineering* **390**. arXiv:2106.07606 [physics], 114474 (Feb. 2022).
10. Krishnapriyan, A., Gholami, A., Zhe, S., Kirby, R. & Mahoney, M. W. Characterizing possible failure modes in physics-informed neural networks. *Advances in Neural Information Processing Systems* **34**, 26548–26560 (2021).
11. Li, Z. *et al.* Physics-Informed Neural Operator for Learning Partial Differential Equations. arXiv:2111.03794 [cs, math] (Nov. 2021).
12. Rosofsky, S. G. & Huerta, E. A. Applications of physics informed neural operators. arXiv preprint arXiv:2203.12634 (2022).
13. Adcock, B., Huybrechs, D. & Martin-Vaquero, J. On the numerical stability of Fourier extensions. *Foundations of Computational Mathematics* **14**, 635–687 (2014).
14. Press, W. H., Teukolsky, S. A., Vetterling, W. T. & Flannery, B. P. *Numerical recipes 3rd edition: The art of scientific computing* (Cambridge university press, 2007).
15. Albin, N. & Bruno, O. P. A spectral FC solver for the compressible Navier–Stokes equations in general domains I: Explicit time-stepping. *Journal of Computational Physics* **230**, 6248–6270 (2011).
16. Fontana, M., Bruno, O. P., Mininni, P. D. & Dmitruk, P. Fourier continuation method for incompressible fluids with boundaries. *Computer Physics Communications* **256**, 107482 (2020).
17. Bruno, O. P. & Paul, J. Two-dimensional Fourier Continuation and applications. *SIAM Journal on Scientific Computing* **44**, A964–A992 (2022).
18. Kovachki, N. *et al.* Neural Operator: Learning Maps Between Function Spaces. arXiv:2108.08481 [cs, math] (Dec. 2021).
19. Li, Z. *et al.* Fourier Neural Operator for Parametric Partial Differential Equations (2020).
20. Li, Z. *et al.* Neural Operator: Graph Kernel Network for Partial Differential Equations. arXiv:2003.03485 [cs, math, stat] (Mar. 2020).
21. Chen, J., Hou, T. Y. & Huang, D. Asymptotically self-similar blowup of the Hou-Luo model for the 3D Euler equations. arXiv preprint arXiv:2106.05422 (2021).
22. Bruno, O. P., Han, Y. & Pohlman, M. M. Accurate, high-order representation of complex three-dimensional surfaces via Fourier continuation analysis. en. *Journal of Computational Physics* **227**, 1094–1125 (Dec. 2007).
23. Luo, G. & Hou, T. Y. Potentially singular solutions of the 3D axisymmetric Euler equations. *Proceedings of the National Academy of Sciences* **111**, 12968–12973 (2014).

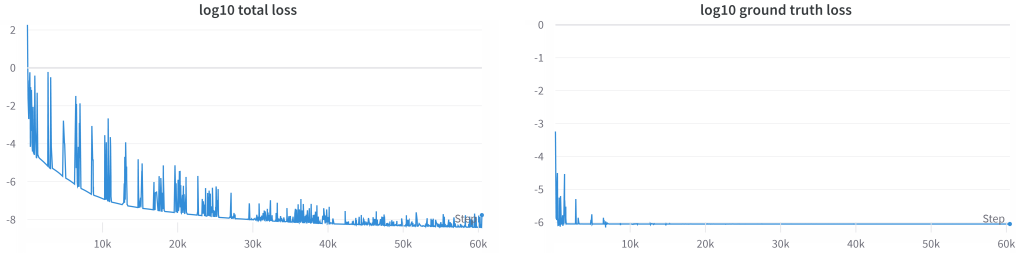


Figure 6: Plots of loss from equation (7) (left) and L^2 loss against exact solution (right) of model 1 when $\lambda = 0.4$. The L^2 loss plateaus almost immediately even though the training loss continues to decrease.

24. Luo, G. & Hou, T. Y. Toward the finite-time blowup of the 3D axisymmetric Euler equations: a numerical investigation. *Multiscale Modeling & Simulation* **12**, 1722–1776 (2014).

A Future Work

A.1 Addressing L^2 Loss Plateau

Despite the promising results shown in section 4.3, there are additional problems to be solved about the effectiveness of these models in learning solutions to differential equations. One problem in particular is the question of whether low loss as computed in equation (7) translates to low L^2 loss of the model output against the exact solution to the differential equation. While training the models presented in this paper, we also tracked the L^2 loss of the model: if u is the model output and f is the exact solution to the differential equation, then this loss is computed as

$$\int_D |f(x) - u(x)|^2 dx.$$

As an example, consider the training process of model 1 for the $\lambda = 0.4$ case as given in section 4. Figure 6 shows the L^2 loss compared against the loss from equation (7). If one trains the model on L^2 loss against the exact solution, then the loss continues to decrease and becomes much lower than the plateau value shown in Figure 6. Additionally, from Table 1, we see that all high-performing models reach the same loss plateaus on $\lambda = 0.4$ and $\lambda = 0.5$. It is unclear why training on equation (7) causes this plateau behavior. Determining why this occurs and how to rectify it is an important subject of future research.

A.2 Differences in Loss Stability During Training

Of the three models described in section 4, Model 1 achieves the lowest loss when trained for 60,000 epochs. However, model 1 also has the least stable loss plot; loss continues to fluctuate even after 60,000 epochs. A comparison of loss plots for each model is shown in Figure 7. One future topic of research would be to determine how the different placements of FC in the PINO model affect loss stability.

A.3 Applications

One long-term goal of the machine learning community is to enable progress on the well-known millennium questions concerning the finite-time blowup of the Navier-Stokes equation [5]. A very important candidate for such a blowup scenario is a self-similar blowup for the axis-symmetric case [23, 24]. It consists of two steps: one first finds an approximate candidate with a specific singular form, and then uses rigorous mathematics to show stability around the equilibrium. Therefore a perturbation around the singularity of the approximate blowup candidate would lead to a finite-time blowup. This procedure requires an extremely high level of accuracy. Many traditional computation methods become infeasible in the fine mesh and high accuracy regime. We aim at tracking numerical candidates using machine learning.

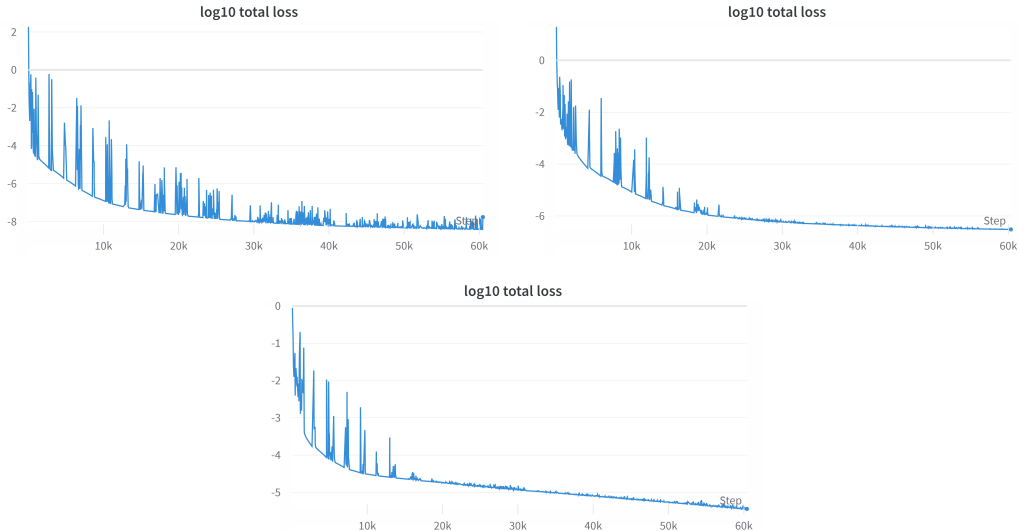


Figure 7: Plots of loss from equation (7) when $\lambda = 0.4$ for models 1 (top left), 2 (top right), and 3 (bottom). Model 1 has the least stable loss despite achieving the lowest loss after 60,000 epochs.

Once a promising candidate model for applying PINO on nonperiodic differential equations is discovered, we can apply it to more complex equations. In particular, transferring these PINO models to 2D and 3D settings would enable the application of more complex equations like the 2D Burgers' equation with viscosity or the Navier-Stokes equation and related models. We have found promising results using FC on one dimension of a 2D fluid blowup problem. Further research in this area will have important implications for fluid blowup research.

B Experiment Parameters

This appendix lists the model hyperparameters and optimization parameters used to train the models in section 4.

Each PINO model has 4 hidden layers (i.e. $L = 4$ in (2)). The first neural network \mathcal{P} is a simple linear layer. The last neural network \mathcal{Q} is two linear layers with a tanh activation in between. The Fourier kernel layers \mathcal{K}_l each use 16 frequency modes for $\lambda = 0.5$ and 32 frequency modes for $\lambda = 0.4$. Each intermediate weight matrix W_l has a width of 200. The model is trained on a uniform grid with 400 grid points.

The training process uses an Adam optimizer with an initial learning rate of 10^{-4} and no weight decay. The scheduler is `ReduceLROnPlateau` with decay factor 0.5, patience 200, threshold 0.0001, and minimum learning rate 0. The model is trained on three 'boundary points': $U(-2) = 1$, $U(2) = -1$, and $U(0) = 0$.

C Additional Model Plots

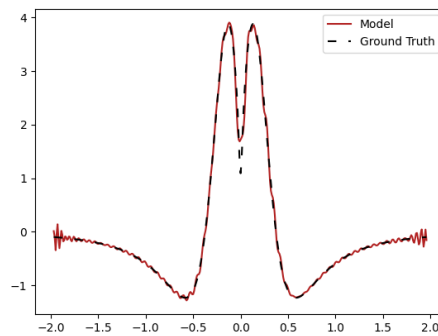


Figure 8: The third derivative of a model using 5th-order Fourier continuation trained on equation (6) for 60,000 epochs, plotted against the ground truth solution. Note the large oscillations at the boundary of the domain.

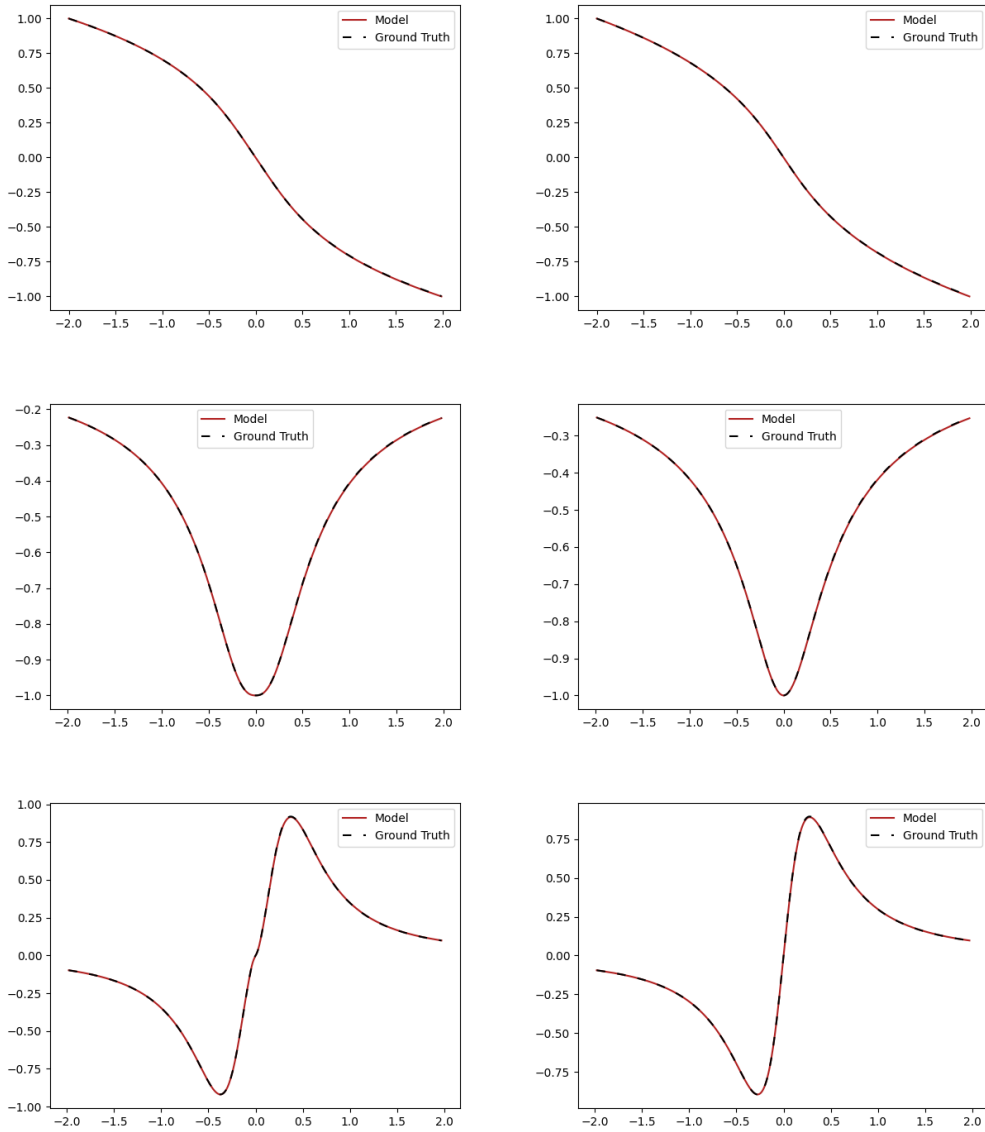


Figure 9: The original model outputs from section 4.3 (top) and their first (middle) and second (bottom) derivatives for $\lambda = 0.4$ (left) and $\lambda = 0.5$ (right). Each model is plotted against the exact solution.